



Microstructure and mechanical properties of ta-C films by pulse-enhanced cathodic arc evaporation: Effect of pulsed current

Jian Hu^a, Qinwen Tian^a, Pengfei Wan^a, Bing Chen^a, Xiubo Tian^{a,*}, Chunzghi Gong^a, Dmitriy A. Golosov^b

^a State Key Laboratory of Advanced Welding and Joining, Harbin Institute of Technology, Harbin 150001, China

^b Thin Film Research Laboratory, Belarusian State University of Informatics and Radioelectronics, Minsk, Belarus

ARTICLE INFO

Keywords:

Ta–C films
Peak current
Pulse-enhanced cathodic arc evaporation
Microstructure
Mechanical properties

ABSTRACT

The ta-C films were fabricated using direct-current cathodic arc evaporation (DC-CAE) and pulse-enhanced cathodic arc evaporation (PE-CAE). The effect of peak currents (I_p) on arc discharge, microstructure and mechanical properties of the films was focused on. The enhanced discharge process, microstructure and mechanical properties of the ta-C films were investigated by means of optical emission spectra (OES), Raman spectroscopy, Nano-indentation, etc. With the same average current, the I_p of 300 A of PE-CAE produced the substrate current of 1.14 A, but a markedly low current (0.82A) was observed for the DC-CAE. The plasma emission intensity of Ar II, C I and C II also increased by about 86%, 66% and 630% at pulse mode. This evidently indicated an enhanced arc discharge by PE-CAE. The highest ratio of CII/ArII (2.98) and electron excitation temperature (1.38 eV) was observed. DC-CAE led to a lower concentration of sp^3 bonding (47.3%, $I_D/I_G = 0.39$) of ta-C films with a thickness of 171 nm. In contrast, the ta-C films fabricated by PE-CAE ($I_p = 300$ A) possessed the smallest I_D/I_G (0.22) as well as the highest concentration of sp^3 bonding (65.1%). The thickness increased by about 30% in comparison with that by DC-CAE. The largest thickness (330 nm) was obtained at the peak current of 200A, mainly relating to the increased evaporation of carbon atom/ions. The hardness evaluated from the ta-C films fabricated by DC-CAE was about 29 GPa. However, the hardness increased significantly to 57 GPa by PE-CAE ($I_p = 300$ A), and the preferable toughness (H/E^* of 0.11 and H^2/E^{*2} of 0.68) was simultaneously achieved.

1. Introduction

Tetrahedral amorphous carbon film (ta-C film) is a hydrogen-free carbon film with the remarkable properties comparable with those of diamond film, such as high hardness, optical transparency, chemical inertness and etc. [1–3]. Significant efforts have been devoted in recent years to the development of ta-C films for a wide range of technological and industrial applications. Some applications of ta-C films lie in their use as protective films over tooling components [4], magnetic hard disks [5] and medical materials [6] are well established.

The ta-C can be fabricated by a number of deposition techniques involving energetic ions or ion beams, such as cathodic arc evaporation (CAE) [7], pulsed laser-deposition (PLD) [8] and mass-selected ion beam (MSIB) [9]. CAE is an efficient technique for the deposition of the ta-C films for various purposes.

The surface properties of ta-C films are strongly depend on their microstructure (ratio of sp^3/sp^2) and even very subtle change in the deposition parameters lead to the variation in the coating properties.

The optimized bias voltage for the deposition of high concentration of sp^3 bond (88%) is 100 V, which is demonstrated by Polo et al. [10]. The dependence of sp^3 content on the deposition temperature is investigated by Chhowalla et al. [11]. A significant decrease of the sp^3 content from 85% to 60% is induced when deposition temperature exceeds 150 °C. As reported by McCann et al., the higher arc current gives rise to the increase of the concentration of sp^3 bonds. The results demonstrate that the ratio of I_D/I_G decreases from 0.28 to 0.16, referring to an increase of sp^3 content, when the arc currents increases from 30 A to 100 A [12]. Strong flux of ions is produced at high arc current. The amount of the amorphous-like structure increases with the incremental ion fluence. However, the maximum arc current is limited by the thermal load on the cathode. The pulsed arc method is characterized by periodic incoming of plasma fluxes to the substrate, consequently, reducing requirements of cooling system [13]. High density and energy of ionized particles are also achieved in the plasma flux [14]. As compared with DC arc, the pulsed character of dense energetic plasma fluxes may result in the changes on the nucleation mechanism

* Corresponding author.

E-mail address: xiubotian@163.com (X. Tian).

<https://doi.org/10.1016/j.diamond.2019.107479>

Received 1 April 2019; Received in revised form 16 July 2019; Accepted 17 July 2019

Available online 18 July 2019

0925-9635/ © 2019 Elsevier B.V. All rights reserved.

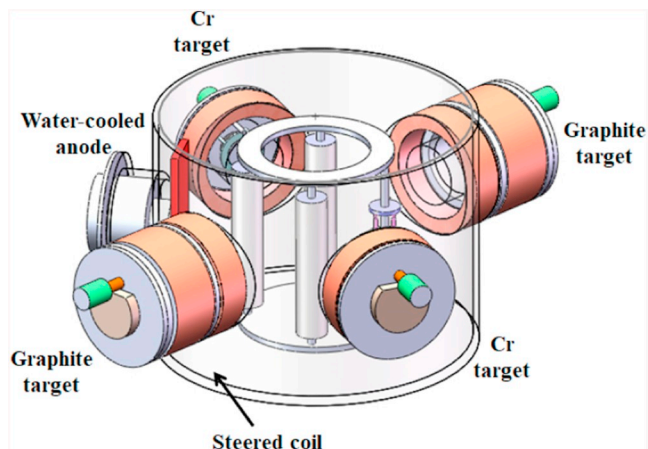


Fig. 1. Global view of the deposition system.

Table 1
Deposition parameters.

Layer		Cr	CrC	ta-C
Gas		Ar	Ar	Ar
Pressure(Pa)		0.4	0.3	0.05
Target current(A) (in DC mode)	Cr cathode	80	70	0
	C cathode	0	80	80
Bias voltage(V)		-200	-70	-100
Bias duty cycle(%)		75	75	75
Time(min)		15	15	50
Peak current (A)	C cathode	0	300	0, 150, 200, 250, 300

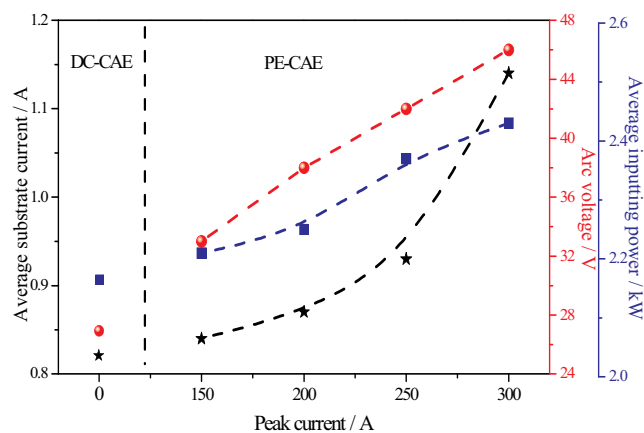


Fig. 2. Average substrate current, average inputting power and arc voltage as a function of the pulse currents.

and the formation of different carbon metastable phases.

Pulse-enhanced cathodic arc evaporation (PE-CAE) has also been utilized to fabricated ta-C films. Zavaleyev et al. have studied the effect of substrate temperature on properties of ta-C films. The decrease of the substrate temperature from 195°C to 67°C lead to the increased content of tetrahedral sp³-bond from 48 to 62% [15]. Panwar et al. and Inkin et al. report the highest concentration of the sp³ bonded carbon may be obtained at a proper bias potential of 40–60 V [5,16], which is a little lower than that used in conventional DC arc (e.g. 100 V) [17]. The deposition temperature and the incident energy are the crucial parameters. Moreover, the amplitude of the peak current is also an important processing parameter during the deposition process. The ion density and the distribution of the ions are significantly influenced by the peak currents [18]. Fuchs et al. [19] demonstrate that the ions

density measured positioned at 0° with respect to the cathode normal direction increases by 23% while decreases by 36% at 45° as the peak currents increase from 150 A to 500 A. Moreover, Ma et al. [20] investigate that the substrate current and the ion species increase sharply as the peak currents increase from 150 A to 400A. However, few investigations have been focused on the influence of peak currents on the arc discharge of graphite as well as the microstructure and surface properties of the tetrahedral amorphous carbon coating.

In this paper, the cathodic arc was operated using a pulsed power supply. The discharge and plasma behavior of pulsed arc were monitored. And the effect of pulsed currents on the microstructure and surface properties of ta-C films was investigated systematically.

2. Experimental procedure

The deposition process of ta-C films was performed in a deposition system with 800 mm in diameter and 600 mm in height as shown in Fig. 1. It was equipped with four cathodic arc sources, as well as one water-cooled anode. Carbon plasmas were generated in a cathodic arc discharge (in pulse mode) with purity of graphite cathode (99.99%). Two opposite chromium targets (99.9%) were used (in DC discharged mode) to deposit the Cr and CrC supporting layers. M2 high-speed steel (W₆Mo₅Cr₄V₂) and single crystal silicon substrates (100) were used as the substrates and cleaned in an ultrasonic bath using alcohol and deionized water. Then the samples were dried in warm air. The samples were placed on a planetary holder with a rotation speed of 3 rpm.

Prior to deposition, the vacuum chamber was pumped down to 6×10^{-3} Pa. The dual etching processes were carried out to improve the adhesion of the subsequently deposited films. The samples were firstly cleaned with a bias voltage of 200 V for 15 min by argon ions generated from the arc-enhanced glow discharge (AEGD) with the current of 50A. During the AEGD process, the discharge was sustained between the shuttered chromium cathode and the water-cooled square anode. Afterwards, the Cr ions were further utilized to enhance the cleaning and activation of the sample surface, and then the under-layers of Cr and CrC were deposited to improve the adhesion between the film and substrate.

During the deposition process of the ta-C films by PE-CAE, the arc was operated with average current of 80A composed of a continuous base current of 50 A superposed with a pulse currents of 150–300A with the same pulse width of 550 μs. The pulse frequency was adjustable to keep a constant average pulsed arc current of 30 A. Tenuous Argon was used to improve working stability of the arc plasma sources. For comparison, the DC-CAE with the current of 80 A was also performed. (See Table 1.)

The surface and cross-sectional morphologies of the films were observed by a field emission scanning electron microscopy (SUPRA 55 SAPHIRE, Germany). The optical emission spectroscopy (OES) was applied to detect the species in the plasma produced by the graphite cathodes during the growth process of the ta-C films. The optical emission spectra (OES) were monitored with multichannel spectrometer AvaSpec-2048FT-4-DT (Avantes, Holland). The spectral resolution was 0.1 nm in the wavelength range of 400–800 nm. The optical spectra were obtained by integrating the optical signal for 300 ms. Background noise was recorded before any spectra was acquired and subtracted from the optical spectra. Raman spectrum (Renishaw inVia, UK) instrument with a wavelength of 532 nm was applied to investigate the chemical bonding of the as-prepared films. All of the measurements were recorded for the wavelength ranging from 800 to 2000 cm⁻¹. The elemental states and chemical compositions of the films were detected via an X-ray photoelectron spectroscopy (XPS) (ESCALAB 250, Thermo Fisher Scientific, USA). Photoelectron emission was excited by monochromatic Al K source with a spot size of 500 μm. The analyzer was operated at 20 eV pass energy for high resolution spectra at a step of 0.1 eV and 100 eV for survey spectra at a step of 1.0 eV. The nano-hardness (H) and Young's modulus (E) were measured using a G200

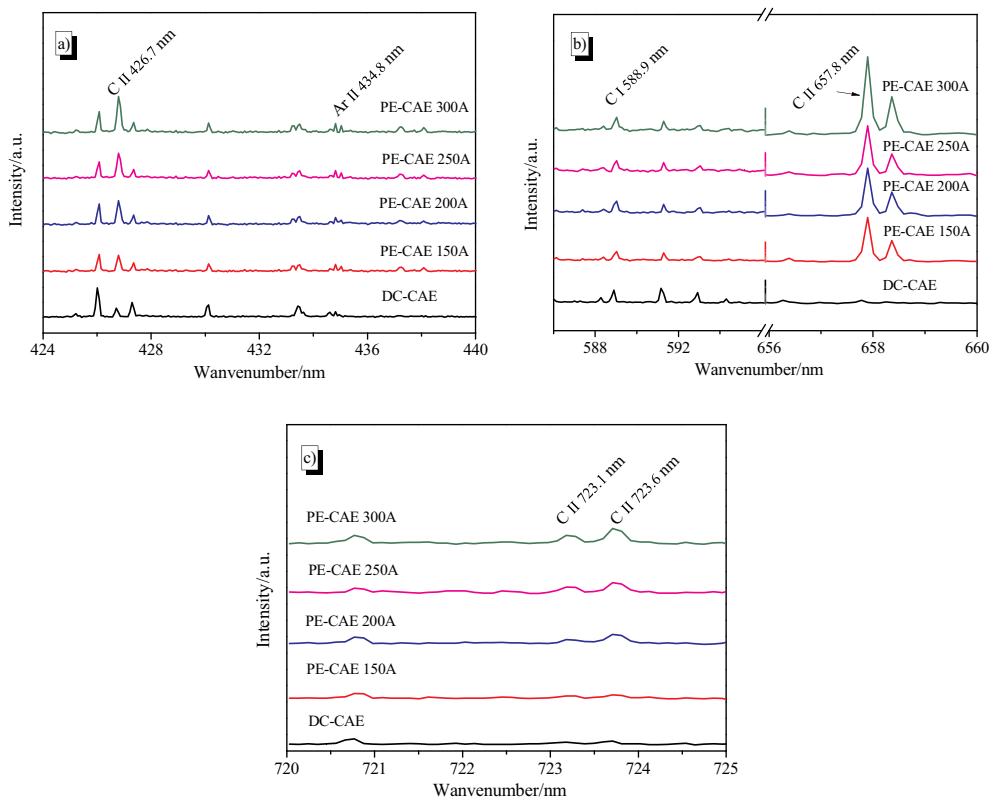


Fig. 3. Optical emission spectra of the plasma at different pulse currents: a) from 424 nm to 440 nm, b) from 586 nm to 660 nm, c) from 720 nm to 725 nm.

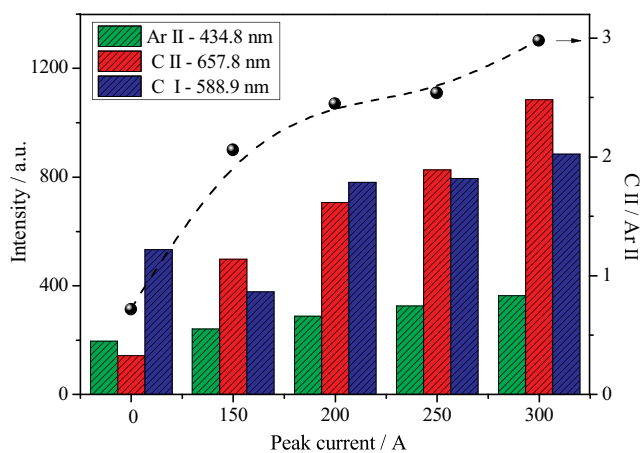


Fig. 4. Emission intensities of ArII, CI and CII species and the ratio of CII/ArII as a function of the pulse currents.

nano-indentation testing system with a standard Berkovich indenter according to the continuous stiffness measurement (CSM). The penetration depth was 1000 nm and the loads varied with the penetration depth, corresponding to the maximum applied load of about 220 mN. The maximum applied load was monitored from the plots which illustrated the load as a function of indentation depth during the tests. The value of H and E were taken from the value of the short platform (about 15 nm) near the highest average value of the detected data to avoid the influence of the macro-particles on the surface and the soft substrate. The measurements were averaged over 5 indents for each sample to improve measurement accuracy. The adhesion strength was evaluated by the Rockwell C (HF) indentation tests using a Rockwell C diamond stylus (cone apex angle 120° and tip radius R of 0.2 mm) at an applied load of 1470 N. After indentation, an optical microscope (Olympus

GX71, Japan) was used to evaluate the test. Friction tests were carried out on a ball-on-disc wear apparatus at room temperature. The rotation speed was 50 rpm with the loading of 50 g. A GCr15 ball steel ball with a diameter of 6 mm was selected as the counterpart.

3. Results and discussion

The average substrate current and arc voltage, as a function of the pulse currents, are shown in Fig. 2. The results showed an increase in the discharge voltage from 27 V to 46 V with the I_p increased to 300 A from 0 A. The inputting power increased simultaneously from 2.16 kW to 2.43 kW. The increase of arc voltage was in agreement with the results obtained by Gan et al. [21], who reported that a rise of arc voltage from 31 to 50 V was observed with the pulse current increased from 80 to 220A. A stable arc discharge required sufficient electrons to transport between the anode and the cathode [22]. As the pulse current increased, more electrons needed to be employed to sustain arc discharge and consequently an increase in the arc voltage had to be induced. The substrate current was directly related to plasma density near the substrates [23]. The substrate current increased by about 39% with the I_p increasing from 0 to 300 A. This indicated an improved plasma density around the substrates, which was attributed to the enhanced ionization by elevated arc voltage and the focusing effect by the pulse currents [18–19]. In contrast to the arc in DC mode, the plasma would extend in all directions from the cathode as demonstrated by Zhang et al. [24]. The constriction of more plasma was induced by pulsed arc (especially higher pulse currents). More carbon ions and electrons would transport to the substrate region, instead of the consumption on the chamber wall. Consequently, the increased number of excited and ionized species by colliding with the neutral particles was generated [25–26]. Actually, from the viewpoint of the inputting energy, larger pulse current also led to the increase of electrical inputting power [27], due to elevated arc voltage. The higher arc voltage accelerated the electrons to a high-energy level, which gave rise to higher ionization efficacy. As

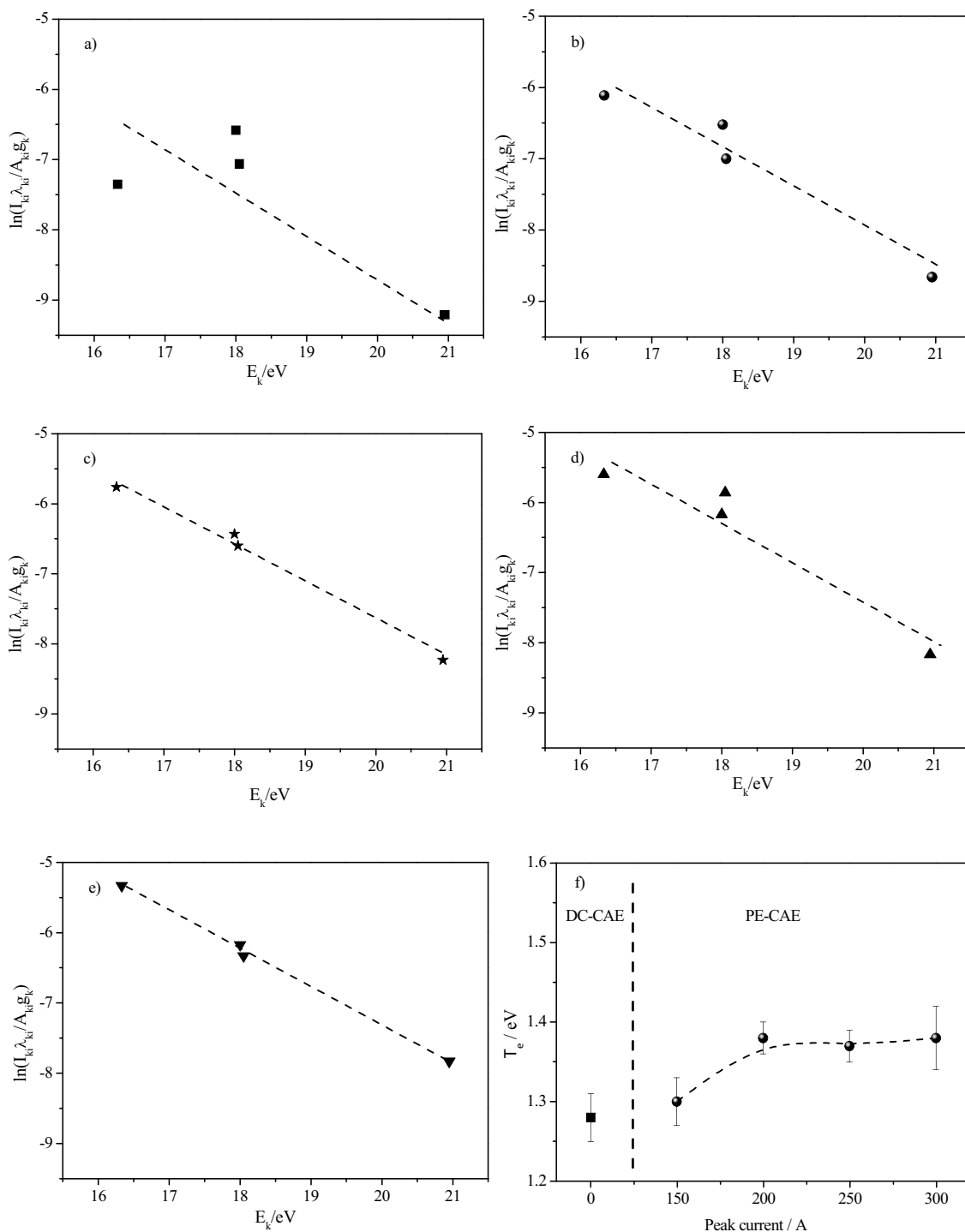


Fig. 5. Boltzmann plot performed at different peak currents: a) DC-CAE and b) 150 A, c) 200 A, d) 250 A, e) 300 A for PE-CAE and f) the electron excitation temperature T_e variation with pulse currents.

a result, a larger average substrate current was obtained.

Fig. 3 depicts a typical OES spectrum of graphite cathodic arc discharge in DC-CAE and PE-CAE mode. The main emission lines in the argon-carbon plasmas were assigned to Ar I and Ar II in the range of the wavelength from 400 to 800 nm. The bands ranging from 650 to 795 nm were mainly assigned to the emissive radiation of the Ar I species. The emissive radiation of the Ar II intensively located at the range from 425 to 500 nm [28]. Furthermore, emission lines located at the wavenumber of 588.9 nm and 657.8 nm corresponded to neutral (C I) and singly ionized carbon (C II), respectively [29–31]. No matter

whether pulse-arc or DC-arc discharge mode, the intensity of Ar I radicals was higher than those of Ar II and C II due to low excitation energy of Ar I (~11.83 eV) [32]. And the excitation energy of Ar II and C II was about 19 eV and 14.5 eV, respectively [29,33]. The emission lines of C I (excitation energy of 10.9 eV) depicted the diminished intensity in comparison with that of Ar I [34]. The carbon atoms were generated from the vapor on the surface of the cathode. Generally, some transport losses occurred when the carbon atoms flew to the substrate [35]. However, the argon atoms were excited not only near the cathode but also on the flight path to the anode. Consequently,

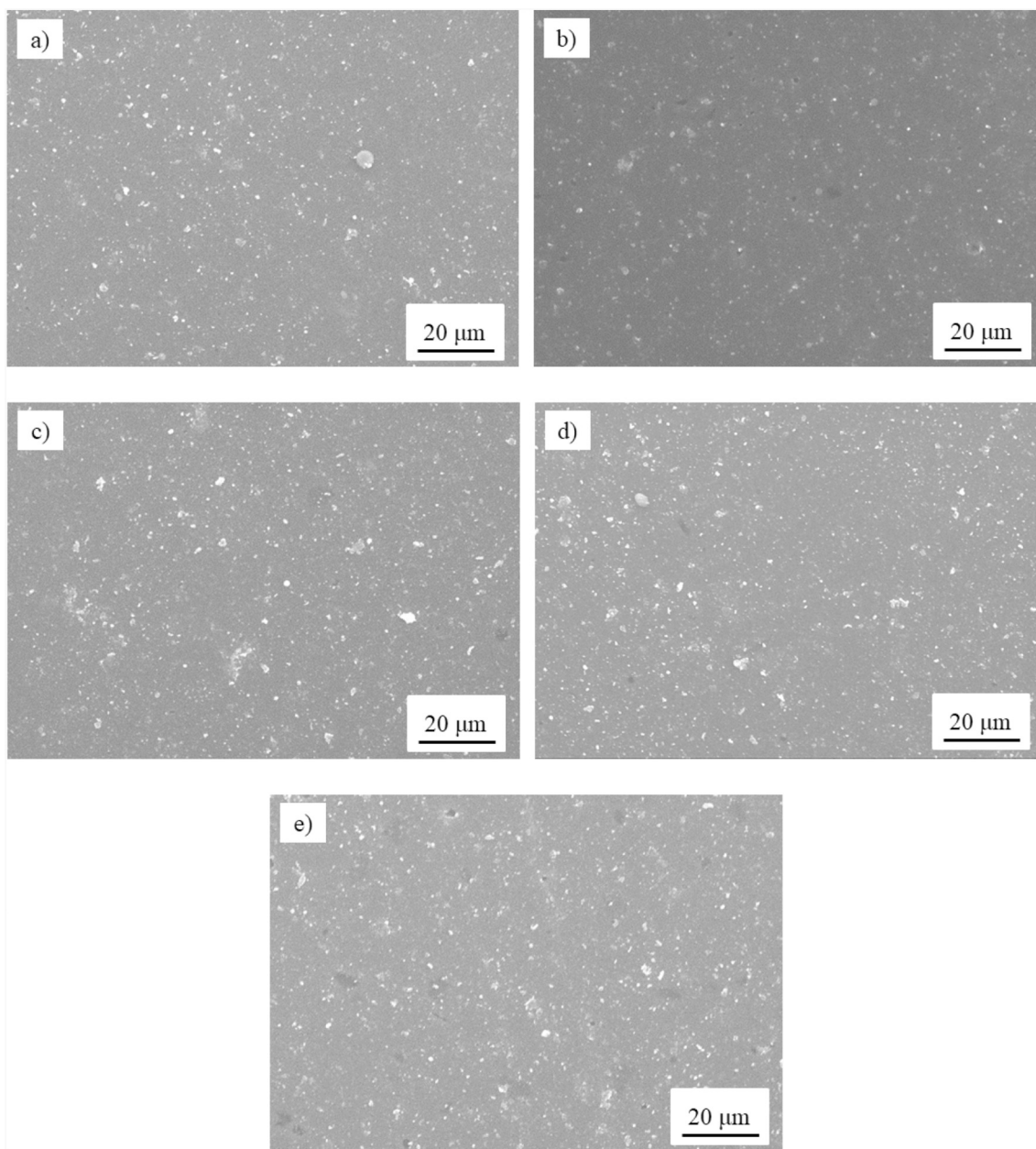


Fig. 6. Surface morphology of ta-C films deposited at different pulse currents a) DC-CAE, PE-CAE: b) 150 A, c) 200 A, d) 250 A and e) 300 A.

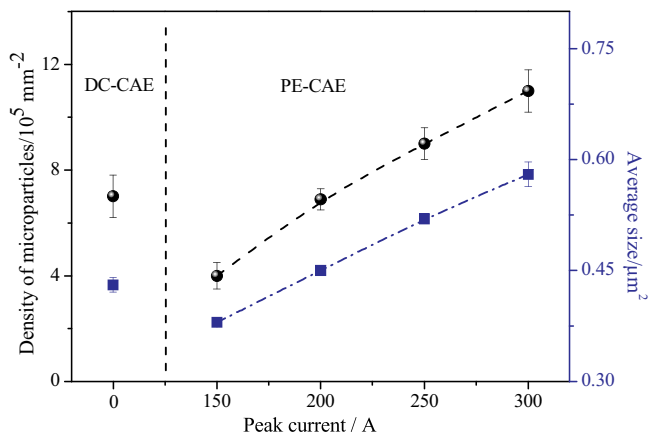


Fig. 7. Density and average size of macroparticles on the surface of ta-C coating.

higher emission intensity of Ar I was detected. Obviously, the emission intensity of Ar I, Ar II, C I and C II lines changed with the discharge mode and the employed pulsed current of I_p . The intensities of Ar I, Ar II, C I and C II lines were considerably higher in the plasma of PE-CAE than those in the plasma of DC. The intensity of C II emission lines increased by the consumption of carbon atoms, result in weak C I emission lines.

The variations of the emission intensities of Ar II (434.8 nm), C I (588.9 nm), C II (657.8 nm) and the ratio of intensity of C II/Ar II versus the pulse currents are shown in Fig. 4. The increase of the pulse currents from 0 to 300 A led to a dramatic increase in the intensity of C II line from 142.8 to 1085. The intensity of Ar II line was simultaneously increased from 196 to 363.5. The emission intensity was utilized to evaluate the number of emission species by Diamant et al. [36] and Zhou et al. [37]. The intensity ratio of the C II (657.8 nm) to Ar II (434.8 nm) was used as an estimate of their relative concentrations in the plasma. The increase in the ratio of C II/Ar II indicated an enhancement of the fraction of the carbon ions in the plasma. The pulse

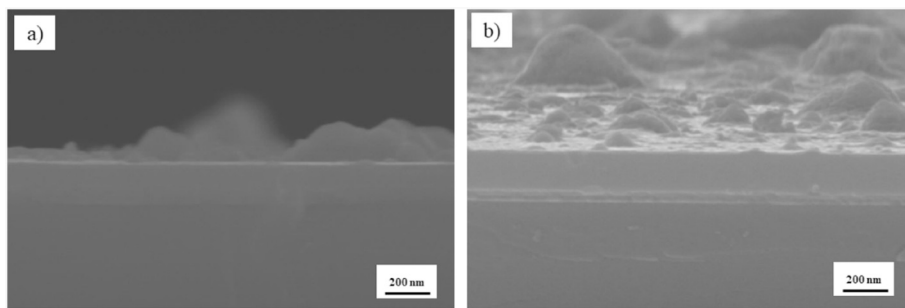


Fig. 8. Fractured cross-section morphologies of ta-C films deposited by a) DC-CAE, b) PE-CAE ($I_p = 300A$).

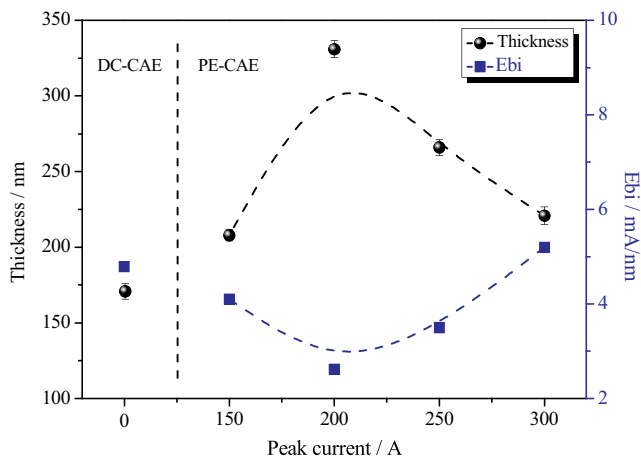


Fig. 9. Thickness of ta-C films and Ebi value deposited at different pulse currents.

current of 300 A led to the largest value of C II/Ar II, which was about 3 times higher than that in DC-CAE process. This might be related to larger arc voltage in pulse arc mode (shown in Fig. 2). Consequently, a higher degree of ionization of the carbon species was induced [27]. Furthermore, the gradual increase in ionization rate of argon might be attributed to higher ionization energy of argon (~19 eV).

The C II lines lied at 426.7 nm, 657.8 nm, 723.1 nm and 723.6 nm were used to calculate the electron excitation temperature T_e . Considering the detected carbon species, these lines had the big difference between their corresponding upper energy levels, and provided the best straight line fit in the Boltzmann plot, which led to better accuracy in T_e determination from the Boltzmann plot [38]. The following relation was used for T_e calculations [39]:

$\ln \frac{I_{ki} \lambda_{ki}^2}{A_{ki} g_k} = \ln \frac{N(T)}{U(T)} - \frac{E_k}{kT_e}$ where, I_{ki} is the integrated line intensity of the transition involving the upper level (k) and the lower level (i), λ_{ki} is the transition wavelength, A_{ki} is the transition probability, g_k is the statistical weight of the level k , $N(T)$ is the total number density, $U(T)$ is

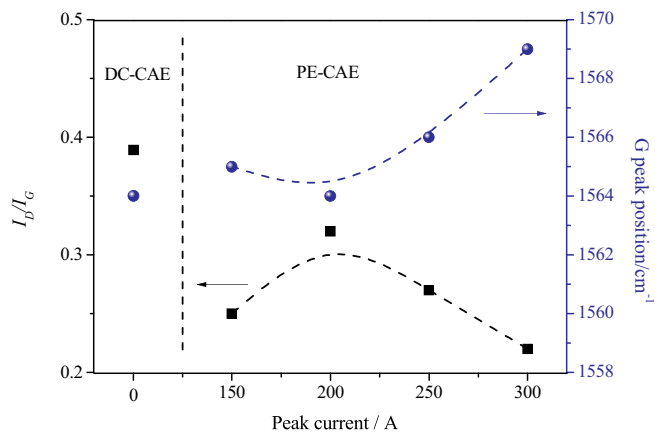


Fig. 11. I_D/I_G ratio and the G peak position as a function of pulse current.

the partition function, E_k is the energy of the upper level, k is the Boltzmann constant, and T_e is the excitation temperature. A plot of $\ln(\lambda I/gA)$ versus the term energy E_k gives a straight line with a slope equal to $-1/kT_e$. The line identifications and different spectroscopic parameters, such as the wavelength λ_{ki} , statistical weight g_k , transition probability A_{ki} , and term energy E_k , are chosen according to Ref. [34]. We assumed that the plasma was in a local thermal equilibrium (LTE) wherein the excitation temperature could be considered to be equal to the electron mean temperature T_e [40]. The linear fitting to the experimental data of the four-point Boltzmann plot are presented in Fig. 5. The scattered data was calculated from the DC-CAE, which may relate to a little lower electron density [41]. The dependence of electron temperature T_e on the pulse current is shown in Fig. 5f). T_e was higher in pulse arc mode than that in DC arc mode, which rose up with the increase of pulse current. At pulse arc mode, T_e increased from 1.28 eV to 1.38 eV as the peak currents increased to 200A from 0A. Afterwards the electron temperature T_e changed slightly. The higher T_e estimated from PE-CAE in comparison with that of DC-CAE may be attributed to the increased discharge power. However, the increase of the peak

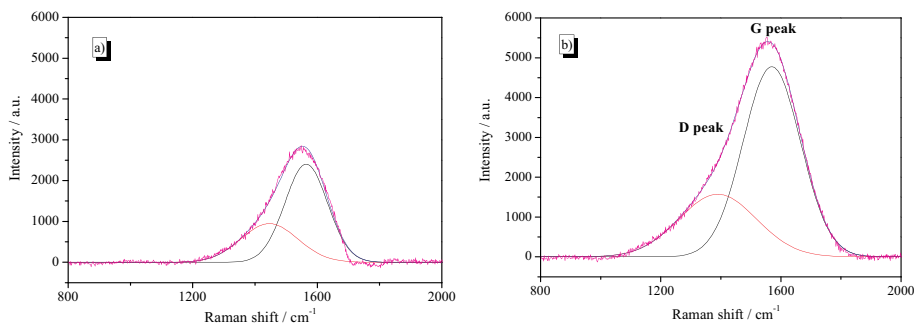


Fig. 10. Raman spectra deconvolution of ta-C films deposited by a) DC-CAE, b) PE-CAE ($I_p = 200A$).

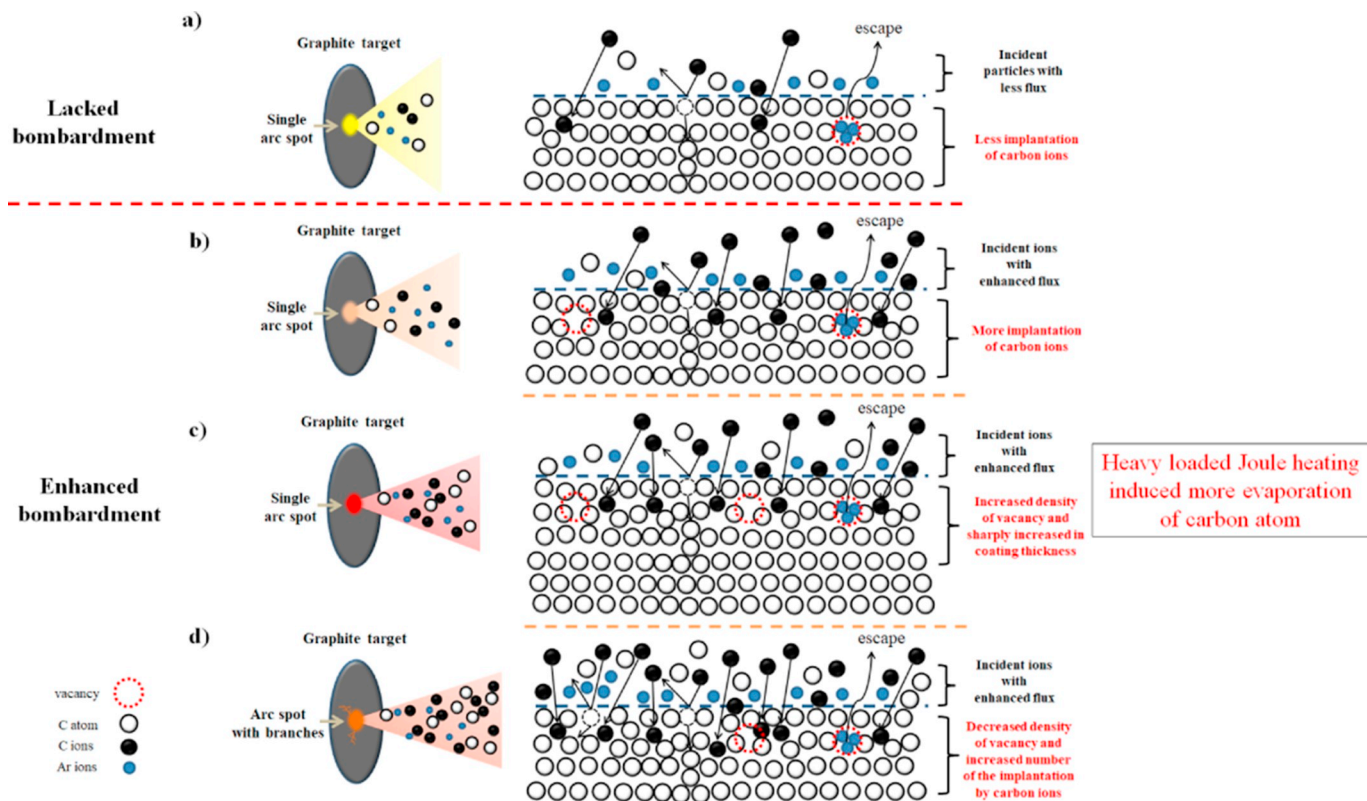


Fig. 12. Schematic illustration of a conjectural growing mechanism of ta-C films at different pulse currents, a) DC-CAE and PE-CAE; b) 150 A, c) 200 A, d) 300 A.

currents from 200 A to 300 A led to a platform value, i.e. around 1.38 eV. In fact the area/number of the arc spots should be taken into account. As reported by Kimblin, there was a limitation current that one arc spot could conduct [42]. The results showed that the maximum current for copper was about 100 A, whereas lower than 20 A for zinc. The refractory materials of carbon exhibited current division with the maximum current per spot of about 200 A. As the peak currents increased to over 200 A, the arc spots on the target surface may split into two or more. The higher inputting power may disperse in larger area of the arc spots. Then, the power loaded on unit area of the arc spot may not increase apparently. Consequently, a platform value of T_e was expected and then a little decreased (as shown in Fig. 5.) as the peak currents increased from 200 A to 300 A.

Surface morphology of ta-C films deposited at different pulse currents is presented in Fig. 6. And the dependence of the number and the average size of macroparticles (defects) on pulse current are displayed in Fig. 7. Many macroparticles were observed on the surface of the ta-C films. The size of most macroparticles was less than $1 \mu\text{m}^2$. It was quite acceptable in wear-resistant films on working parts of friction surfaces and instruments [43]. The macroparticles with large size were rarely observed. According to the results shown in Fig. 7, the density and the average size of macroparticles were $7 \times 10^5 \text{mm}^{-2}$ and $0.43 \mu\text{m}^2$, respectively, for DC-CAE samples. However, they were decreased to $4 \times 10^5 \text{mm}^{-2}$ and $0.38 \mu\text{m}^2$, respectively, by superposing a pulsed current of 150 A. The reduction of the macroparticles for PE-CAE may be attributed to fewer macroparticles ejected from the cathode. The pulse arc led to a higher spot velocity in comparison with DC arc, which may be reasonable for the reduction of macroparticles [21]. The higher rotational velocity resulted in a shorter period in the existence of the spots on local places, which avoiding the overheating of local places and resulting in the reduction of the occurrence of macroparticles on the cathode surface [44]. Meanwhile, the stripping effect induced by the increased incident ions may also contribute to the reduction of macroparticles. As the superposed pulse current was used, the average

substrate current was increased (shown in Fig. 2). The increased bombardment to macroparticles led to the removal of loosely bounded macro-particles [45]. Consequently, fewer macroparticles were observed at the pulse current of 150 A.

Further increment of the pulse current led to the increase in the emission of macroparticles. The pulse current of 300A produced the density and the size of macroparticles of $11 \times 10^5 \text{mm}^{-2}$ and $0.58 \mu\text{m}^2$, respectively. A higher pulse current indicated a larger inputting power to the carbon arc. Apart from the rotational velocity of arc spots, the inputting power also had an effect on the density of the macroparticles. Higher rotational velocity of arc spots was achieved by increasing the pulse current. However, the spots moved still rather slowly over the graphite cathode surface in comparison with the metal cathode (such as copper, etc.) [46]. Unlike most materials, the electrical resistivity of carbon decreased with temperature. This, coupling with the porous nature of most commonly available graphite cathodes, resulted in arc spots moving more slowly across the cathode surface [47]. The increased inputting power was simultaneously obtained on the carbon target surface at higher I_p , resulting in heavy Joule heating on the cathode. The increased Joule heating, coupling with the small velocity of arc spots, resulted in increased volume of molten materials at the cathode spots. The number as well as the size of macroparticles emitted from the cathode spot was increased [48]. From the viewpoint of the etching effect induced by argon ions, the increased peak current also led to the decreased concentration of argon ions in the plasma, shown in Fig. 4. The loosely bounded macro-particles could not be scrubbed away immediately, in spite of the higher plasma density near the substrate [49]. Consequently, larger density as well as the increased size of macroparticles appeared on the surface of as-deposited ta-C films at higher I_p . The pulsing parameters should be optimized to decrease the density and size of macroparticles.

The cross-sectional SEM micrographs of ta-C films are shown in Fig. 8. The ta-C films displayed a relatively dense and structure-less morphology. The thickness of the ta-C films deposited in DC mode was

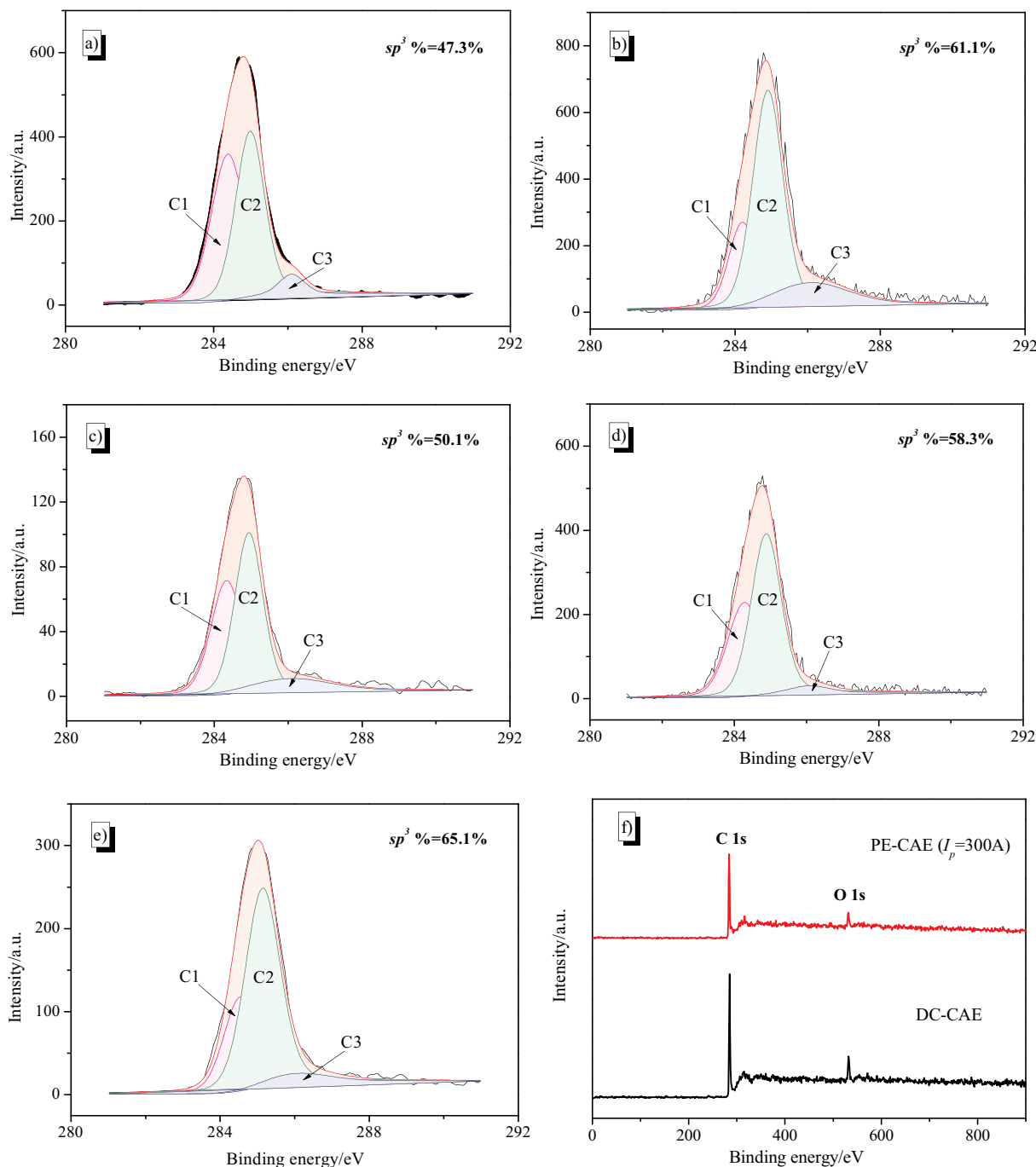


Fig. 13. Deconvoluted C1s spectra versus binding energy of as-deposited ta-C films, a) DC-CAE, PE-CAE: b) 150A, c) 200A, d) 250A, e) 300 A, and f) the general XPS scan of ta-C films deposited in both discharge mode.

much less than that deposited in the pulse mode (shown in Fig. 9). This was attributed to that the larger amount of carbon species was produced by the larger inputting power to target and the focusing effect induced by the pulse currents. More carbon atom/ions in the focused plasma column transported from the region near the cathode to the substrates. The larger coating thickness was achieved [50–51].

The pulse current of 200 A led to a sharp increase in coating thickness. As the peak current of 200 A was applied, the increased Joule heating was loaded in one melting pool on the cathode surface resulting in intensive increase in the evaporation of the carbon. As shown in Fig. 4, the emission intensity of carbon atoms was increased by nearly 110% as compared to that of 150A, in addition to the increased number of carbon ions. More carbon could escape from the cathode and

transport to the work piece, resulting in the increase in the coating thickness [52]. Meanwhile, a lower value of E_{bi} was calculated, relating to the increased density of vacancy produced by the energetic argon ion. As mentioned by Rossi [53], the effect of vacancy production on the structure of carbon films was considerable at high incident energy of argon ions, i.e. ~ 100 eV. The increased amount of argon ions was obtained resulting in more vacancies. Consequently, a looser structure was produced [54]. But with increasing the pulse current to 300A, a lower coating thickness accompanied by a higher value of E_{bi} was obtained. When the pulse currents were higher than 200A, a possible formation of branches of the arc spots should be taken into account [55]. As demonstrated by Kimblin, the maximum current per spot for carbon was about 200 A [42]. Consequently the increased Joule heating

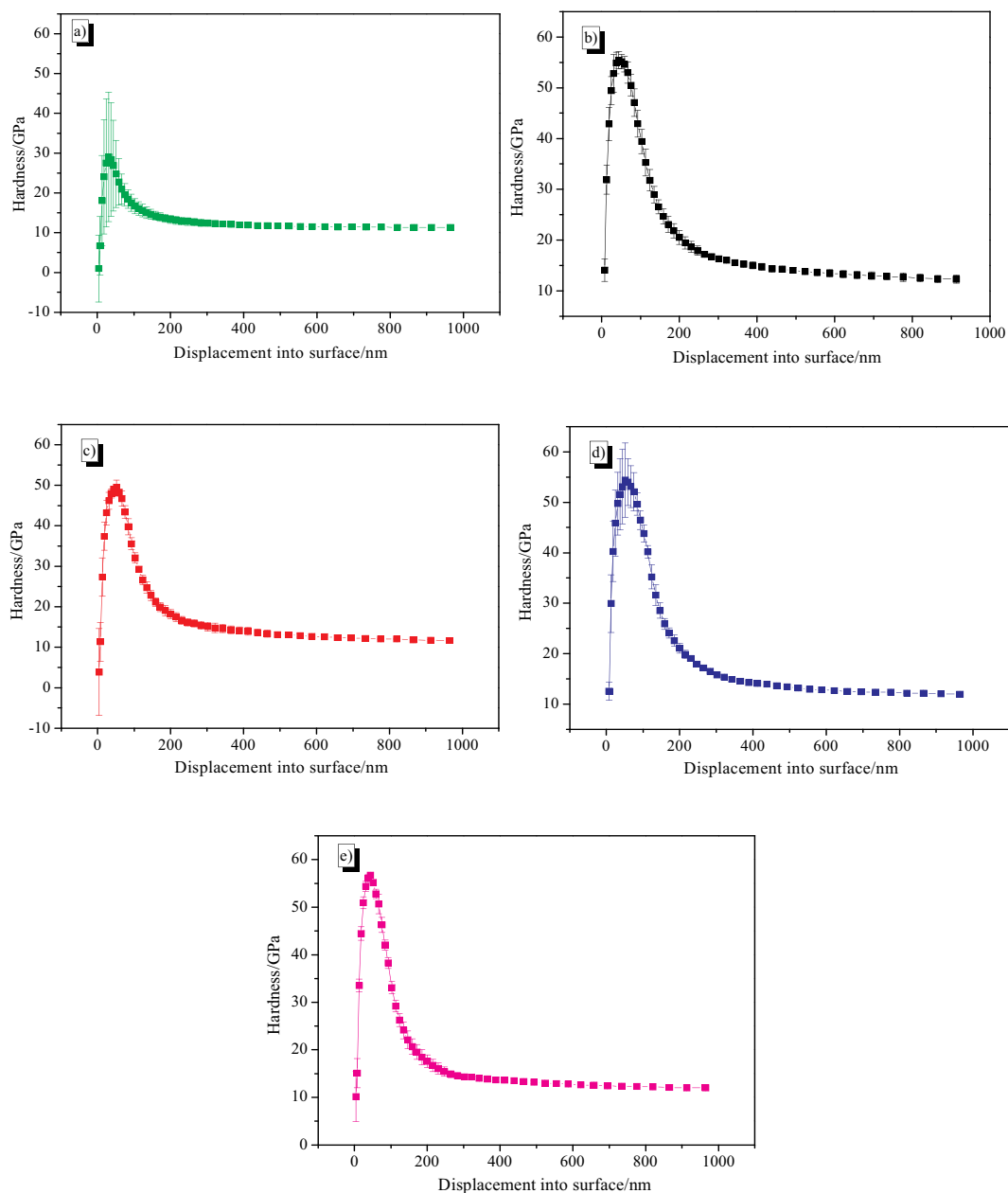


Fig. 14. Hardness of ta-C films deposited at different pulse currents a) DC-CAE, PE-CAE: b) 150 A, c) 200 A, d) 250 A and e) 300 A.

was loaded separately in the different melting pool. And the evaporation rate of carbon atoms does not increase evidently. Nevertheless, higher plasma density and higher incident flux of ions still occur at higher peak current. This led to the increased bombardment on the substrates, which increased the mobility of the adatom significantly [56]. The highly mobile adatom may move or diffuse to the sites of the produced vacancy. The vacancy could also be padded by knocking the surface carbon atoms to the vacancy existing in the sub-layer. Meanwhile, re-sputtering effect of ion bombardment became considerable at higher ion flux. Therefore, a denser structure (e.g. higher Ebi) and reduced thickness were achieved [57–58].

Raman spectroscopy was used to investigate the vibrational modes of carbon atoms due to chemical bonding. In the higher wavenumber, the broad feature in the 1100–1800 cm^{-1} region was related to the vibrational modes of graphitic characteristics in diamond like carbon, generally consisting of G and D bands locating at around 1580 cm^{-1} and around 1350 cm^{-1} , respectively. The deconvolution of the as-deposited ta-C films deposited in both modes are depicted in Fig. 10. Two

separated peaks were obtained. The maximum peak was corresponded to the G-band locating at around 1564 cm^{-1} , which was different from that of polycrystalline graphite locating at about 1580 cm^{-1} . In general the intensity ratio of G-band to D-band (I_D/I_G) was correlated to the sp^3 bonding content [59], as shown in Fig. 11. Higher I_D/I_G of 0.39 was evaluated for DC-CAE in comparison with that obtained by PE-CAE. For PE-CAE, The I_D/I_G ratio for the ta-C films increased markedly from 0.25 to 0.32 when the pulse current was increased from 150 A to 200 A. A further drop of the I_D/I_G ratio to 0.22 was observed as the pulse current increased to 300 A. The change in the pulse current from 150 A to 300 A had no significant effect on the shift of the G peak position. The pulse current of 300 A led to the highest value of 1569 cm^{-1} . The main change, i.e., the increase of the G-peak position, was caused by the change of sp^2 configuration from rings to olefinic groups, with their higher vibrational frequencies lying above the band limit of graphite. This effect was larger than the downwards tendency of the G peak position due to mix with lower-frequency sp^3 modes [60].

The structure of the ta-C films were determined by many factors

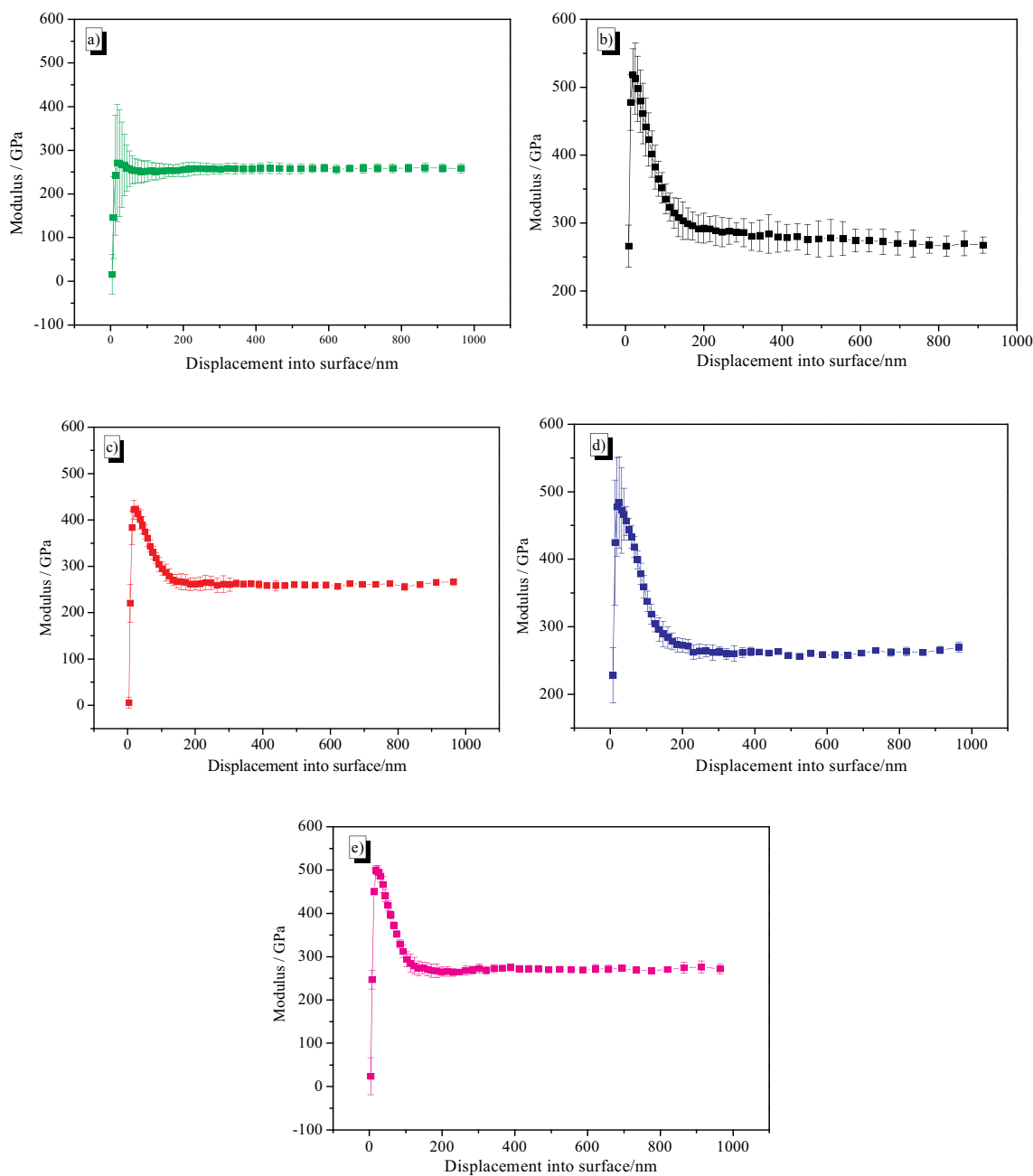


Fig. 15. Modulus of ta-C films deposited at different pulse currents a) DC-CAE, PE-CAE: b) 150 A, c) 200 A, d) 250 A and e) 300 A.

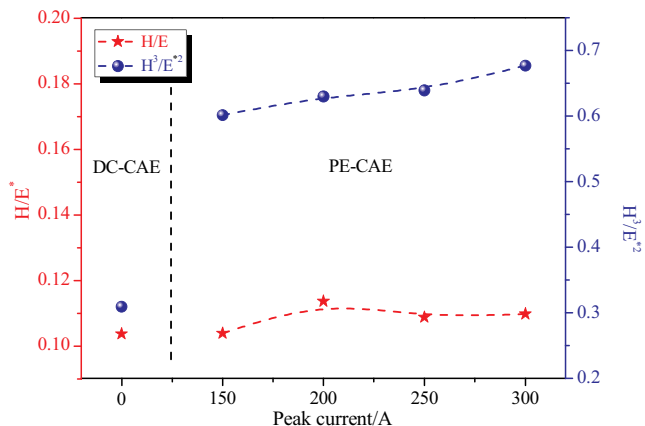


Fig. 16. H/E^* and H^3/E^{*2} of ta-C films deposited at different pulse currents.

such as energy of incident ions, ion flux, ratio of ion to atom, processing temperature, etc. For thin films, the high-density layer was sandwiched between the low-density sp^2 layers at the interface (between the buffer layer and the bottom region of the ta-C layer) and the surface, which might have the effect of decreasing the overall ratio of sp^3/sp^2 bonds in the films [61–63]. This was consistent with the results of McCann et al. [12]. The ratio of I_D/I_G decreased monotonously from 0.39 to 0.25 as the film thickness of the ta-C increased from 30 nm to 100 nm, indicating an increase in the ratio of sp^3/sp^2 bonds.

In fact even the film thickness is the similar, the structure of the ta-C films may also be different. As indicated in Fig. 9, the film thickness obtained at the peak current of 300 A was about 220 nm which was similar to that of 150 A (208 nm). However the peak current of 300 A led to a much lower ratio of I_D/I_G (Fig. 11) and a higher fraction of sp^3 bonds (Fig. 13) and smaller sp^2 clusters in the films [64–66]. An important effect, which was the bombardment by the incident particles,

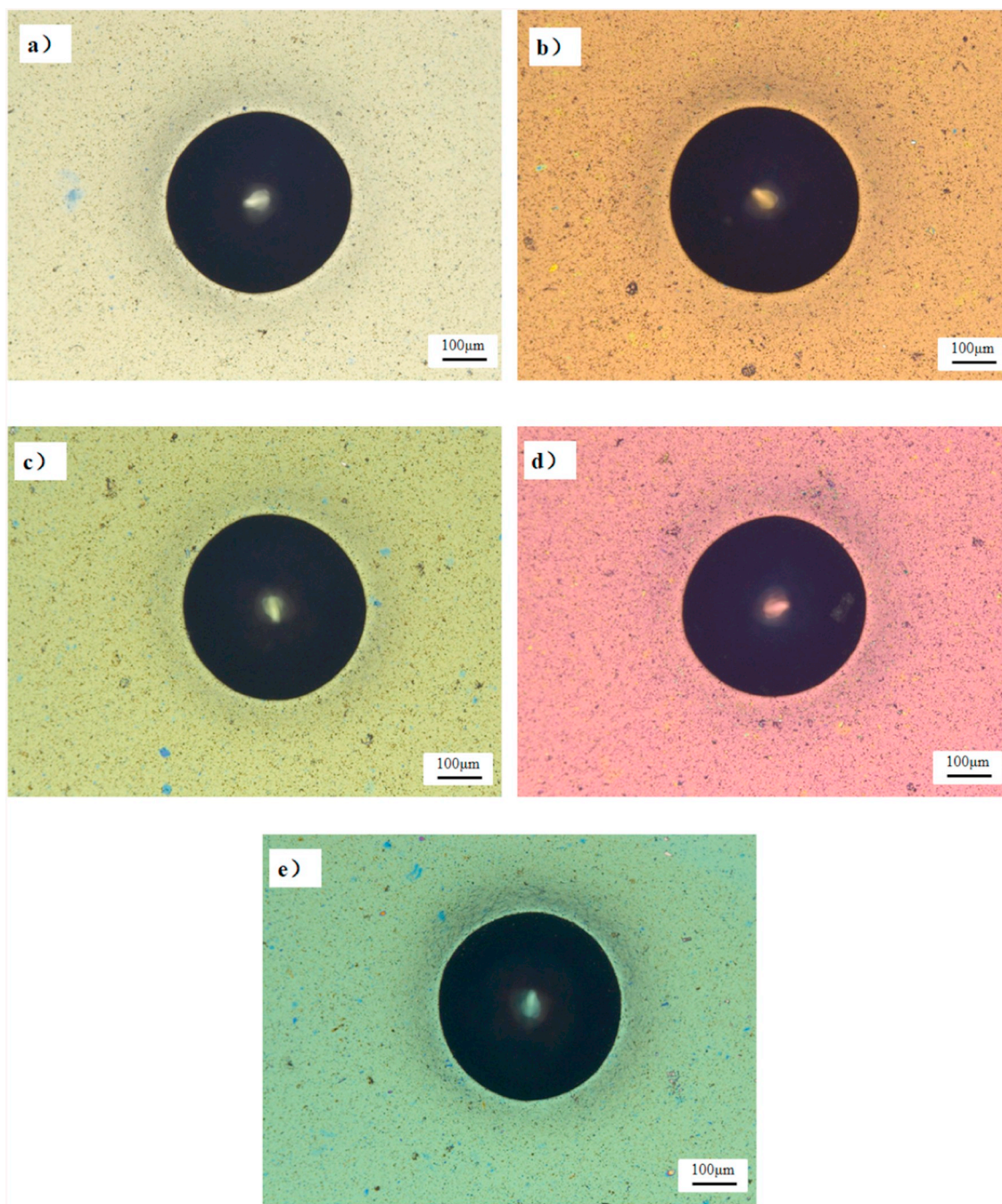


Fig. 17. Optical microscopy images of ta-C films deposited at different pulse currents after Rockwell-C indentation tests at 150 kgf, a) DC-CAE, PE-CAE; b) 150A, c) 200 A, d) 250 A and e) 300A.

should be taken into account. The ion peening model employed by Robertson was frequently utilized to describe the growth process of the ta-C films [67–68]. As shown in Fig. 12, incident carbon ions with sufficient energy penetrated the atomic surface layer generating sp^3 bonding. As the pulse current increased to 300 A, larger number of carbon ions was produced, resulting in intensive bombardment on the substrate, which was responsible for much more disorder in the films. The increase of disorder produced cross linking between graphitic planes by sp^3 bonds which could explain the observed increase in the corresponding sp^3 concentration at the pulse current of 300 A (shown in Fig. 12d)). This strongly disordered phase grew at the expense of the sp^2 bonded domains, and reduced their size [52]. With the similar thickness, the film by peak current of 300A possessed the denser structure

and more concentration of sp^3 bonds. However, the concentration of the sp^3 bonds was not increased continuously as the peak current increased from 150 A to 300 A. The pulse current of 200 A led to the unexpected degradation of the sp^3 bonds in the films in comparison with that of 150 A. With respect to the unfiltered deposition process, a distinctive increase in the evaporation of carbon atoms might explain this degradation of the sp^3 bonds (Fig. 4). The number of carbon atoms increased more rapidly than that of carbon ions. As depicted in Fig. 12c), the number of carbon atoms participated in the growth of the ta-C films increased dramatically, which led to the insufficient conversion from sp^2 to sp^3 bonds. Moreover, the higher density of vacancies might be produced by the increased amount of energetic argon ions at 200 A, resulting in looser structure than that at 150 A. The sites

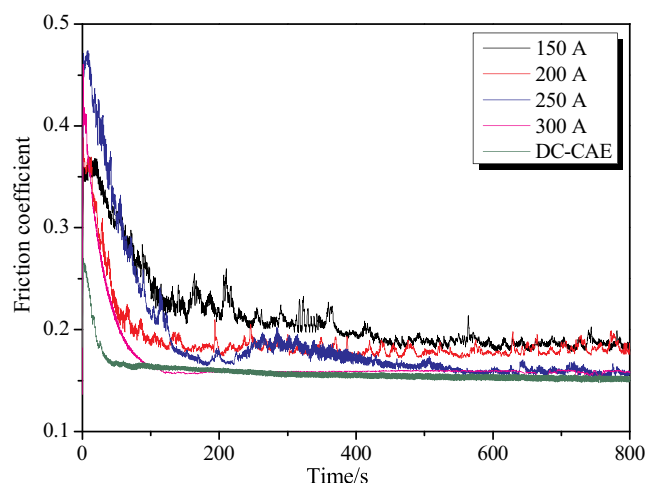


Fig. 18. Friction coefficients of the ta-C films at different peak currents.

of the vacancies offered the channels for the relaxation of the compressive stress, which promoted the transition from sp^3 to sp^2 bonding [69]. Consequently, the less concentration of sp^3 bonding was obtained at the peak current of 200 A.

X-ray photoelectron spectroscopy (XPS) has been used to evaluate the concentration of sp^3 bonding in ta-C films directly [3]. The general XPS scan and the deconvoluted C1s spectra of the ta-C films deposited at different pulse currents both in pulsed and direct current mode are displayed in Fig. 13. The observed peaks located at ~ 284 eV and ~ 532 eV were assigned to carbon and oxygen, respectively [70]. The oxygen in the both films may be attributed to the long time exposure of the films with atmosphere [71]. The sp^3 fraction of DLC film can be deduced from XPS fitting for C 1s core peak, consisting of peaks corresponding to C1 (sp^2 , ~ 284.3 eV), C2 (sp^3 , ~ 285.0 eV), and C3 (C–O contaminated, ~ 286.1 eV) [72–74]. As illustrated in Fig. 13, the dependence of the concentration of sp^3 bonding on the pulse current is similar to that for I_D/I_G . The PE-CAE produced higher fraction of sp^3 bonding in the ta-C films than that of DC-CAE (e.g. 47.3%). For PE-CAE, the minimum value was evaluated at the pulse current of 200 A (e.g. 50.1%). The largest concentration of sp^3 bonding in the ta-C coating was obtained at the pulse current of 300 A (e.g. 65.1%). The result is consistent with that deposited by Han [75], who prepare ta-C coating using the filtered cathodic vacuum arc technique. In their work, the deduced concentration of sp^3 bonding is about 70% and the ratio of I_D/I_G is 0.24 (similar to our research).

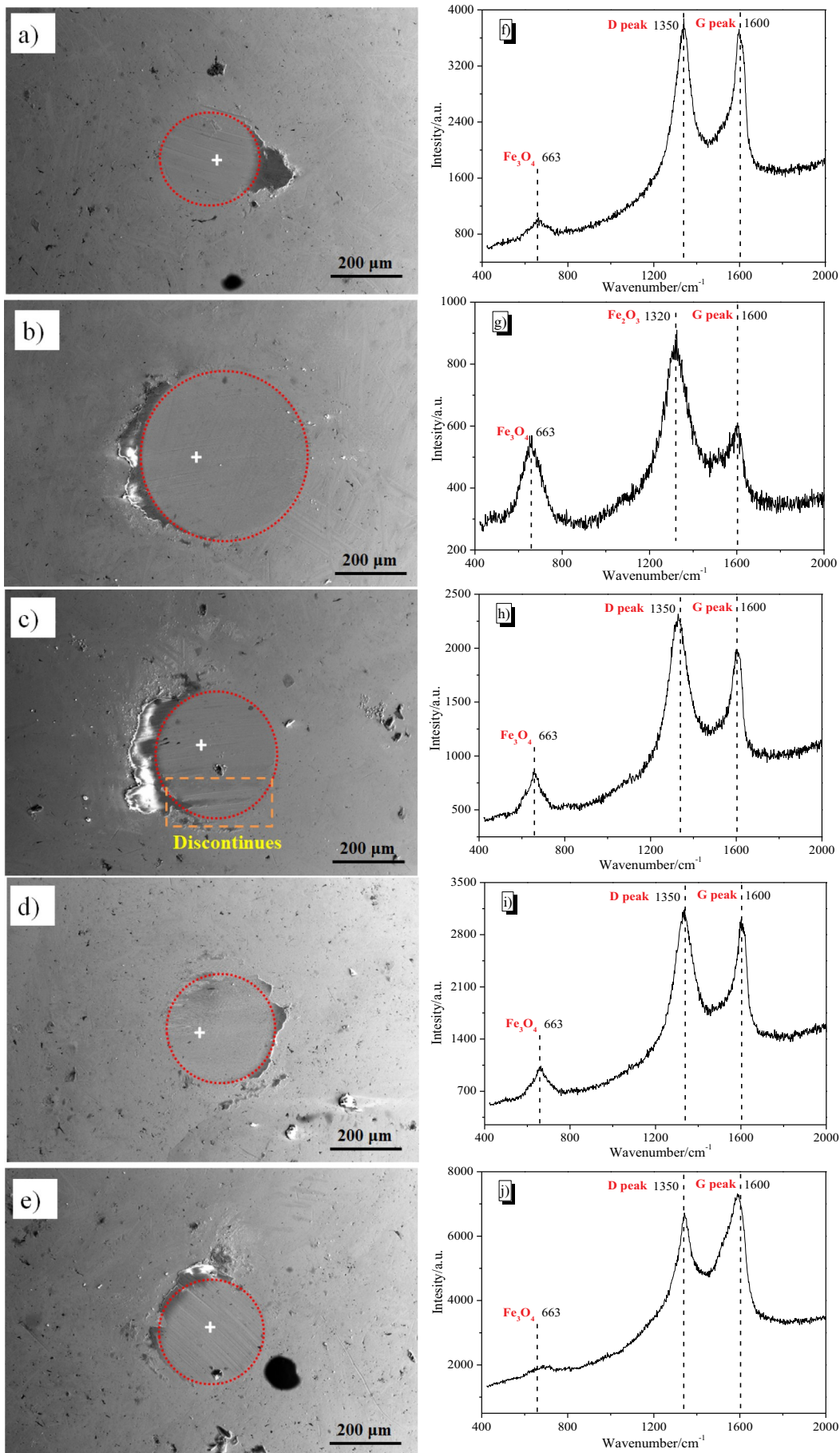
The dependence of the hardness (H), and modulus (E) on the pulse current is presented in Fig. 14 and Fig. 15. The hardness of ta-C coating deposited in DC mode was about 29 GPa, while the hardness of ta-C films deposited by PE-CAE ranged from around 49 GPa to 57 GPa. The surface properties of the ta-C films were determined by many factors such as sp^3/sp^2 bonds, thickness, etc. The residual stress of hard carbon films would accumulate gradually with the increase of the film thickness [76]. This might favor for the increase of hardness. As a result, the larger film thickness produced by PE-CAE led to higher hardness than that of DC-CAE. This was consistent with that of Makowski et al. [77]. The thicker films ($2.7 \mu\text{m}$) led to the higher hardness (61 GPa) than that of the thinner one ($1.4 \mu\text{m}$, 51 GPa). By increasing the peak current to 300 A, higher hardness was obtained in comparison with that of 150 A with similar film thickness. The increased film hardness was likely associated with the upgrade of the sp^3 bonds in the films by the increased peak current [78–79]. The denser structure and more concentration of sp^3 bonds were achieved by the heavy bombardment of the carbon ions at the peak current of 300 A. The structure with higher density could carry more loads, contributing to the higher hardness [80].

As depicted in Fig. 16, the value of H^3/E^{*2} was significantly higher for PE-CAE than that for DC-CAE. Where E^* is defined as effective

Young's modulus ($E^* = E/(1 - \nu^2)$) and ν is Poisson's ratio. The highest value of H^3/E^{*2} ratio and the relatively higher value of H/E^* for the ta-C coating were found to be 0.68 and 0.11, respectively, at the pulse current of 300A. This indicated a higher toughness [81–82]. Toughness could be enhanced if crack initiation and propagation were hindered. The Raman spectra have demonstrated the evidence of the microstructure constituted of smaller graphitic clusters embedded in a strongly disordered mixture of sp^2 and sp^3 hybridized carbon for PE-CAE in comparison with that of DC-CAE. This may led to the increase of boundary complicity in PE-CAE films. Usually, the cracks propagated along the weak region, in most cases, the region boundaries. Therefore, hindrance of crack propagation could be realized by strengthening grain boundary and increasing boundary complicity. And the ta-C coatings by PE-CAE possessed high resistance to the crack or weak crack propagation [83].

The adhesion between the substrate and film was evaluated from the radial and lateral cracks around the indentation after Rockwell-C tests shown in Fig. 17. The damage of the coating was compared with the well-known adhesion strength quality scheme according to VDI guidelines 3198 (1991), where HF1 indicated excellent adhesion and HF6 very poor adhesion [82]. The films deposited by DC-CAE exhibit excellent adhesive strength HF1 (no cracks and delamination). The pulse currents from 150A to 300A led to the similar adhesion of HF1. At a close look of indentation, the pulse current increased to 200A and 250A resulted in the slight deterioration of the film away from indentation edge. It was attributed to the defects (vacancy) produced by the argon. The indentation-induced cracks may then propagate along these defects and could result in coating delamination [84]. In fact, pulse mode led to larger thickness and higher microhardness of the ta-C, still demonstrating the adhesion of HF1. This evidently displayed those films possessed a higher resistance of the coating to de-bonding or spalling, referring to the decreased density of vacancy and the preferable toughness [85].

Fig. 18 shows the friction coefficient (COF) of the ta-C films. At the beginning, the coefficient of friction was higher and then decreased gradually. This was attributed to the running-in of the film and counterpart and consisted of abrasion, chipping or tearing off from the film of macroparticles. Afterwards the films were polished with uniform abrasion [86]. The film by DC-CAE showed the smallest friction coefficient (~ 0.148). The highest friction coefficient was about 0.181 (at 150 A) and then decreased to 0.155. The friction coefficient of ta-C films might be related to the graphitization of the films, carbonic transfer layer formed on the contacting surfaces during sliding and the macroparticles on the film surface [87–88]. The lower friction coefficient of the ta-C films fabricated by DC-CAE mainly derived from the higher concentration of sp^2 bonds and the formation of graphitization transfer layer during sliding progress [89]. In contrast, the lower concentration of sp^2 bonds for PE-CAE led to higher COF. The samples fabricated with peak current of 300 A produced the higher concentration of sp^3 bonds (65.1%). However, the COF was lower than that at 150 A. In addition to the effect of higher hardness, the graphitic macroparticles on the film surface should be taken into account. The counterpart (GCr 15) might be worn out easily due to the massive disparity of the hardness between the counterpart (around 10 GPa) and the as-deposited ta-C films (more than 50 GPa) [90–91]. It was supposed that the 'soft' macro-particles might be torn off easily and absorbed on the surface of the counterpart, forming the transfer layer. As the peak current increased to 300 A, higher density of macro-particles was observed. This may favor for the establishment of the transfer layer on the GCr 15, leading to lower COF. It might be supported by the comparison of the surface morphology of the wear scars on the GCr 15 balls as well as the structure of the transition layer formed on the wear scars. The wear surface morphology of the steel balls sliding against the ta-C films under various peak currents is shown in Fig. 19a) to e). The transfer layer seemed to be continuous for all GCr 15 balls, except the discontinuous one at the peak current of 200 A. The structural



(caption on next page)

Fig. 19. SEM images of the wear scars and Raman spectra of transfer layers formed on the GCr 15 balls, a)/f) DC-CAE, PE-CAE: b)/g) 150 A, c)/h) 200 A, d)/i) 250 A and e)/j) 300 A.

characteristics of the transfer layer were further investigated by Raman spectra as shown in Fig. 19f) to j). Two noticeable features could be observed in the Raman spectra of the transfer layer originated from the ta-C film. One was the peak at 663 cm^{-1} which was related to the appearance of Fe_3O_4 , and the other was the appearance of a pronounced D peak at 1350 cm^{-1} and G peak at 1600 cm^{-1} , which was the typical feature of polycrystalline graphite [60]. However, the spectrum of wear track of the ball after sliding on the film obtained at the peak current of 150 A was dominated by the Fe_3O_4 and Fe_2O_3 which was evidenced by a strong peaks at 663 cm^{-1} and 1320 cm^{-1} [92]. In contrast the wear track of the ball against the film by peak current of 300A was featured by strong spectrum of polycrystalline graphite meaning more transfer layer.

4. Conclusion

The effect of pulse currents on the enhanced discharge, micro-structure and mechanical properties of tetrahedral amorphous carbon (ta-C) fabricated by PE-CAE and DC-CAE ($I_p = 0\text{ A}$) have been investigated. The DC-CAE plasma contained a small flux of C II and Ar II, while the PE-CAE plasma demonstrated a great increase in the flux of C II, in addition to more amount of Ar II. The pulse current of 300A produced the largest substrate current (1.14 A), the highest ratio of C II/Ar II (2.98) and electron excitation temperature (1.38 eV) as well. At the same average current, the ta-C coating by DC arc mode possessed a smaller thickness and less concentration of sp^3 bonding (47.3%), with a hardness of about 29 GPa. The increased ions flux in the PE-CAE mode resulted in increased coating thickness, higher concentration of sp^3 bonding, in addition to the larger hardness. PE-CAE mode also produced higher toughness (H/E^* of 0.11 and H^3/E^{*2} of 0.68). The pulse current of 300 A fabricated the ta-C coating with the highest concentration of sp^3 bonding (65.1%) and hardness (57 GPa). It was attributed to the plasma focusing effect and ionization enhancement effect induced by the high pulse currents. The COF for PE-CAE (0.158 for 300 A) was higher than that of DC-CAD (0.145). The pulse current of 200A produced a higher deposition rate due to the increased amount of evaporated carbon atoms by intensive Joule heating at local arc spot. Afterwards the evaporation effect decreases at every arc spot due to the fact that the maximum current per spot for carbon was about 200 A. Therefore, a higher superposed pulse current should be employed, which is beneficial for controllable movement of arc spot, higher plasma density, better microstructure and optimal mechanical properties of ta-C films.

Acknowledgements

The authors gratefully acknowledge the financial support of this research from National Natural Science Foundation of China (Nos. 11675047, 11875119, 51811530059).

References

- [1] M. Fazio, D. Manova, D. Hirsch, E. Valcheva, A. Kleiman, S. Mändl, A. Márquez, Depth-resolved study of hydrogen-free amorphous carbon films on stainless steel, *Diam. Relat. Mater.* 74 (2017) 173–181.
- [2] L.Y. Huang, J.W. Zhao, K.W. Xu, J. Lu, A new method for evaluating the scratch resistance of diamond-like carbon films by the nano-scratch technique, *Diam. Relat. Mater.* 11 (2002) 1454–1459.
- [3] V. Zavaleyev, J. Walkowicz, T. Kuznetsova, T. Zubar, The dependence of the structure and mechanical properties of thin ta-C coatings deposited using electromagnetic venetian blind plasma filter on their thickness, *Thin Solid Films* 638 (2017) 153–158.
- [4] Y. Fujii, T. Imai, Y. Miyamoto, N. Ueda, M. Hosono, T. Harigai, Y. Suda, H. Takikawa, H. Tanoue, M. Kamiya, M. Taki, Y. Hasegawa, N. Tsuji, S. Kaneko, Dry machining of metal using an engraving cutter coated with a droplet-free ta-C film prepared via a T-shape filtered arc deposition, *Surf. Coat. Technol.* 307 (2016) 1029–1033.
- [5] O.S. Panwar, B. Deb, B.S. Satyanarayana, M.A. Khan, R. Bhattacharyya, A.K. Pal, Characterization of as grown and nitrogen incorporated tetrahedral amorphous carbon films deposited by pulsed unfiltered cathodic vacuum arc process, *Thin Solid Films* 472 (2005) 180–188.
- [6] G. Chen, Z.Y. Wang, H. Wang, X.L. Zhao, J. Hu, S.H. Wang, S.F. Zhang, Effects of tetrahedral amorphous carbon film deposited on dental cobalt-chromium alloys on bacterial adhesion, *Surf. Coat. Technol.* 206 (2012) 3386–3392.
- [7] L.H. Li, J.Z. Tian, X. Cai, Q.L. Chena, M. Xua, Y.Q. Wu, R.K.Y. Fu, P.K. Chu, Influence of ion energies on the surface morphology of carbon films, *Surf. Coat. Technol.* 196 (2005) 241–245.
- [8] P. Tian, X. Zhang, Q.Z. Xue, Enhanced room-temperature positive magnetoresistance of a-c:Fe film, *Carbon* 45 (2007) 1764–1768.
- [9] G. Fanchini, S.C. Ray, A. Tagliaferro, V.M. Tiainen, T. Sajavaara, Effect of isotopic substitution on IR and ESR properties of mass selected ion beam deposited ta-C films, *Diam. Relat. Mater.* 12 (2003) 900–904.
- [10] M.C. Polo, J.L. Andújar, A. Hart, J. Robertson, W.I. Milne, Preparation of tetrahedral amorphous carbon films by filtered cathodic vacuum arc deposition, *Diam. Relat. Mater.* 9 (2000) 663–667.
- [11] M. Chhowalla, J. Robertson, C.W. Chen, S.R.P. Silva, C.A. Davis, G.A.J. Amaratunga, W.I. Milne, Influence of ion energy and substrate temperature on the optical and electronic properties of tetrahedral amorphous carbon (ta-C) films, *J. Appl. Phys.* (1) (1997) 139–145.
- [12] R. McCann, S.S. Roy, P. Papakonstantinou, G. Abbas, J.A. McLaughlin, The effect of thickness and arc current on the structural properties of FCVA synthesised ta-C and ta-C:N films, *Diam. Relat. Mater.* 14 (2005) 983–988.
- [13] A. Anders, A review comparing cathodic arcs and high power impulse magnetron sputtering (HIPIMS), *Surf. Coat. Technol.* 257 (2014) 308–325.
- [14] T. Witke, T. Schuelke, B. Schultrich, P. Siemroth, J. Vetter, Comparison of filtered high-current pulsed arc deposition (Φ -HCA) with conventional vacuum arc methods, *Surf. Coat. Technol.* 126 (2000) 81–88.
- [15] V. Zavaleyev, J. Walkowicz, G. Greczynski, L. Hultman, Effect of substrate temperature on properties of diamond-like films deposited by combined DC impulse vacuum-arc method, *Surf. Coat. Technol.* 236 (2013) 444–449.
- [16] V.N. Inkin, G.G. Kirpilenko, A.J. Kolpakov, Internal stresses in ta-C films deposited by pulse arc discharge method, *Diam. Relat. Mater.* 10 (2001) 1103–1108.
- [17] J.H. In, Y.B. Kim, Y. Hwang, J.H. Choi, Control of residual stress of tetrahedral amorphous carbon thin film deposited on dielectric material by filtered cathodic vacuum arc source by using mid-frequency pulse bias voltage, *Surf. Coat. Technol.* 349 (2018) 909–916.
- [18] H. Fuchs, H. Mecke, M. Ellrodt, Distribution of ion current density in a modified pulse arc process as a function of pulse parameters, *Surf. Coat. Technol.* 98 (1998) 839–844.
- [19] H. Fuchs, B. Engers, E. Hettkamp, H. Mecke, J. Schultz, Deposition rate and thickness uniformity of thin films deposited by a pulsed cathodic arc process, *Surf. Coat. Technol.* 142–144 (2001) 655–660.
- [20] Y. Ma, C. Gong, Q. Tian, P.K. Chu, Discharge and plasma characteristics of pulse-enhanced vacuum arc evaporation (PEVAE) for titanium cathode, *IEEE Trans. Plasma Sci.* 99 (2018) 1–7.
- [21] B.K. Gan, M.M.M. Bilek, D.R. McKenzie, P.D. Swift, G. McCreddie, Optimizing the triggering mode for stable operation of a pulsed cathodic arc deposition system, *Plasma Sources Sci. Technol.* (4) (2003) 508–512.
- [22] W.C. Lang, J.Q. Xiao, J. Gong, C. Sun, R.F. Huang, L.S. Wen, Study on cathode spot motion and macroparticles reduction in axisymmetric magnetic field-enhanced vacuum arc deposition, *Vacuum* 84 (2010) 1111–1117.
- [23] P.J. Kelly, R.D. Arnell, The influence of magnetron configuration on ion current density and deposition rate in a dual unbalanced magnetron sputtering system, *Surf. Coat. Technol.* 108 (1998) 317–322.
- [24] T. Zhang, J. Hou, B. Tang, T.K. Kwok, Z. Zeng, I.G. Brown, P.K. Chu, The effect of mesh anode on cathodic arc in focusing magnetic field, *Chinese Phys* 9 (2000) 279–283.
- [25] A. Anders, J. Brown, A plasma lens for magnetron sputtering, *IEEE Trans. Plasma Sci.* 39 (2011) 2528–2529.
- [26] J. Ramm, M. Ante, T. Bachmann, B. Widrig, H. Brändle, M. Döbeli, Pulse enhanced electron emission (P3e™) arc evaporation and the synthesis of wear resistant Al-Cr-O coatings in corundum structure, *Surf. Coat. Technol.* 202 (2007) 876–883.
- [27] M. Buschel, W. Grimm, Influence of the pulsing of the current of a vacuum arc on rate and droplets, *Surf. Coat. Technol.* 142–144 (2001) 665–668.
- [28] D.R. Lide, *CRC Handbook of Chemistry and Physics*, Internet Version 2005, <http://www.hbcpnetbase.com> CRC Press, Boca Raton, FL, 2005, pp. 1480–1490.
- [29] R. Sanginés, C.S. Aké, H. Sobral, M. Villagrán-Muniz, Time resolved optical emission spectroscopy of cross-beam pulsed laser ablation on graphite targets, *Phys. Lett. A* 367 (2007) 351–355.
- [30] J.C. Orianges, C. Champeaux, A. Catherinot, Th. Merle, B. Angleraud, Pulsed laser deposition of tetrahedral amorphous carbon films from glassy carbon and graphite targets: a comparative study, *Thin Solid Films* s453–454 (2004) 285–290.
- [31] M. Hanif, M. Salik, F. Arif, Spectroscopic study of carbon plasma produced by the first (1064 nm) and second (532 nm) harmonics of Nd:YAG laser, *Plasma Phys. Rep.* 3 (2015) 274–280.
- [32] W. Gajewski, A.P. Ehasarian, M. Żelechowski, P.E. Hovsepian, Composition and dynamics of high power impulse magnetron discharge at W-Mo-C target in argon atmosphere, *Surf. Coat. Technol.* 327 (2017) 185–191.
- [33] P. Jamroz, W. Zyrnicki, Optical emission spectroscopy study for nitrogen-acetylene-argon and nitrogen-acetylene-helium 100kHz and dc discharges, *Vacuum* 84 (2010) 940–946.
- [34] NIST Database, <http://physics.nist.gov/PhysRefData/ASD/index.html>.

- [35] J. Vetter, 60 years of DLC coatings: historical highlights and technical review of cathodic arc processes to synthesize various DLC types, and their evolution for industrial applications, *Surf. Coat. Technol.* 257 (2014) 213–240.
- [36] R. Diamant, E. Jimenez, E. Haro-Poniatowski, L. Ponce, M. Fernandez-Guasti, J.C. Alonso, Plasma dynamics inferred from optical emission spectra, during diamond-like thin film pulsed laser deposition, *Diam. Relat. Mater.* 8 (1999) 1277–1284.
- [37] Z.Y. Zhou, G.C. Chen, B. Li, S.J. Askari, W.Z. Tang, C.M. Li, J.H. Song, Y.M. Tong, F.X. Lu, Application of optical emission spectra in controlling dominant crystalline surface of diamond films deposited by DC arc plasma jet CVD, *Surf. Coat. Technol.* 201 (2007) 4987–4990.
- [38] O. Balki, M.M. Rahman, H.E. Elsayed-Ali, Optical emission spectroscopy of carbon laser plasma ion source, *Opt. Commun.* 412 (2018) 134–140.
- [39] M. Hanif, M. Salik, F. Arif, Spectroscopic study of carbon plasma produced by the first (1064 nm) and second (532 nm) harmonics of Nd:YAG laser plasma, *Phys. Rep.* 3 (2015) 274–280.
- [40] U. Helmersson, M. Lattemann, J. Bohlmark, A.P. Ehasarian, J.T. Gudmundsson, Review ionized physical vapor deposition (IPVD): a review of technology and applications, *Thin Solid Films* 513 (2006) 1–24.
- [41] F.J. Gordillo-Vázquez, A. Perea, A.P. McKiernan, C.N. Afonso, Electronic temperature and density of the plasma produced by nanosecond ultraviolet laser ablation of LiF, *Appl. Phys. Lett.* 86 (2005) 181501.
- [42] C.W. Kimblin, Erosion and ionization in the cathode spot regions of vacuum arcs, *J. Appl. Phys.* (7) (1973) 3074–3081.
- [43] V. Zavaleyev, J. Walkowicz, D.S. Aksyonov, A.A. Luchaninov, E.N. Reshetnyak, V.E. Strel'nitskij, Properties of DLC coatings deposited by DC and DC with superimposed pulsed vacuum arc, *Plasma Sources Sci. Technol.* 6 (2014) 237–240.
- [44] G.H. Kang, H. Uchida, B.S. Koh, A study on the surface structure of Ti cathode and the macroparticle of TiN films prepared by the arc ion plating process, *Surf. Coat. Technol.* 86–87 (1996) 421–424.
- [45] Y. Kong, X. Tian, C. Gong, Q. Tian, D. Yang, M. Wu, M. Li, D.A. Golosov, Microstructure and mechanical properties of Ti-Al-Cr-N films: Effect of current of additional anode, *Appl. Surf. Sci.* 483 (2019) 1058–1068.
- [46] L.H. Li, Y. Zhu, F.S. He, D.D. Dun, F. Li, P.K. Chu, J.Z. Li, Control of cathodic arc spot motion under external magnetic field, *Vacuum* 91 (2013) 20–23.
- [47] D.M. Sandersa, A. Anders, Review of cathodic arc deposition technology at the start of the new millennium, *Surf. Coat. Technol.* 133–134 (2000) 78–90.
- [48] Y. Hu, L. Li, H. Dai, X. Li, X. Cai, P.K. Chu, Effects of pulse parameters on macroparticle production in pulsed cathodic vacuum arc deposition, *Surf. Coat. Technol.* 201 (2007) 6542–6544.
- [49] B. Warcholinski, A. Gilewicz, J. Ratajski, Z. Kuklinski, J. Rochowicz, An analysis of macroparticle-related defects on CrCN and CrN coatings in dependence of the substrate bias voltage, *Vacuum* 86 (2012) 1235–1239.
- [50] G. Fedosenko, J. Engemann, D. Korzec, Deposition of diamond-like carbon films by a hollow cathode multi-jet rf plasma system, *Surf. Coat. Technol.* 133–134 (2000) 535–539.
- [51] X.L. Pang, H.L. Peng, H.S. Yang, K.W. Gao, X.L. W, A.A. Volinsky, Fast deposition of diamond-like carbon films by radio frequency hollow cathode method, *Thin Solid Films* 534 (2013) 226–230.
- [52] Z. Li, J.J. Huang, Z.Z. Zhang, F.X. Zhao, Y. Wu, Preparation of high purity nanosilicon powders by direct current arc plasma evaporation method, *Mat. Sci. Eng. B* 229 (2018) 6–12.
- [53] F. Rossi, B. Andre, A.V. Veen, P.E. Mijnders, H. Schut, M.P. Delplancke, W. Gssiler, J. Haupt, G. Lacazeau, L. Abello, Effect of ion beam assistance on the microstructure of nonhydrogenated amorphous carbon, *Nucl. Instr. and Meth. in Phys. Res. B* 206 (2003) 522–526.
- [54] J.R. Hahn, H. Kang, Spatial, Distribution of defects generated by hyperthermal Ar⁺ impact onto graphite, *Surf. Sci.* 446 (2000) L77–L82.
- [55] E. Restrepo, L.A. Garcia, J.J. Castro, A. Devia, Craters formation in a graphite cathode produced by pulsed arc at low pressure, *Appl. Surf. Sci.* 252 (2005) 1276–1282.
- [56] F. Uslu, M. Wuttig, J. Alami, K. Sarakinos, On the relationship between the pulse target current and the morphology of chromium nitride thin films deposited by reactive high power pulsed magnetron sputtering, *J. Appl. Phys. D: Appl. Phys.* 42 (7) (2009) 15304–15310.
- [57] M.C.R. Guimaraes, B.C.N.M. Castilho, T.S. Nossa, P.R.T. Avila, S. Cucatti, F. Alvarez, J.L. Garcia, H.C. Pintoa, On the effect of substrate oscillation on CrN coatings deposited by HiPIMS and dcMS, *Surf. Coat. Technol.* 340 (2018) 112–120.
- [58] V.D. Ovcharenko, A.S. Kuprin, G.N. Tolmachova, I.V. Kolodiy, A. Gilewicz, O. Lupicka, J. Rochowicz, B. Warcholinski, Deposition of chromium nitride coatings using vacuum arc plasma in increased negative substrate bias voltage, *Vacuum* 117 (2015) 27–34.
- [59] C. Srisang, P. Asanithi, K. Siangchaew, A. Pokaipisit, P. Limsuwan, Characterization of SiC in DLC/a-Si films prepared by pulsed filtered cathodic arc using Raman spectroscopy and XPS, *Appl. Surf. Sci.* 258 (2012) 5605–5609.
- [60] A.C. Ferrari, J. Robertson, Interpretation of Raman spectra of disordered and amorphous carbon, *Phys. Rev. B* 61 (2000) 14095–14107.
- [61] J. Hu, X. Tian, H. Liu, C. Gong, Q. Tian, M. Wu, M. Li, Enhanced discharge and microstructure of the ta-C coatings by electromagnetically enhanced cathodic arc at argon atmosphere, *Surf. Coat. Technol.* 365 (2019) 227–236.
- [62] K. Huang, L.M. Luo, X. Zan, Q. Xu, D.G. Liu, X.Y. Zhu, J.G. Cheng, Y.C. Wu, Microstructure and damage behavior of W-Cr alloy under He irradiation, *J. Nucl. Mater.* 501 (2018) 181–188.
- [63] S. Samad, K.S. Loh, W.Y. Wong, T.K. Lee, J. Sunarso, S.T. Chong, W.R.W. Daud, Carbon and non-carbon support materials for platinum-based catalysts in fuel cells, *Int. J. Hydrog. Energy* 43 (2018) 7823–7854.
- [64] R.M. Dey, D. Patil, S. Kulkarni, Integrated characterization study of diamond like carbon (DLC) synthesized by 2.45 GHz microwave electron cyclotron resonance (ECR) plasma CVD, *Surf. Coat. Technol.* 328 (2017) 30–43.
- [65] S. Neuville, A. Matthews, A perspective on the optimization of hard carbon and related coatings for engineering applications, *Thin Solid Films* 515 (2007) 6619–6653.
- [66] S. Praver, K.W. Nugent, Y. Lifshitz, G.D. Lempert, E. Grossman, J. Kulik, I. Avigal, R. Kalish, Systematic variation of the Raman spectra of DLC films as a function of sp²:sp³ composition, *Diam. Relat. Mater.* 5 (1996) 433–438.
- [67] S. Xu, B.K. Tay, H.S. Tan, L. Zhong, Y.Q. Tu, S.R.P. Silva, W.I. Milne, Properties of carbon ion deposited tetrahedral amorphous carbon films as a function of ion energy, *J. Appl. Phys.* 79 (1996) 7234–7240.
- [68] A.C. Ferrari, J. Robertson, Resonant Raman spectroscopy of disordered, amorphous, and diamond like carbon, *Phys. Rev. B* 64 (2001) 075414-1–075414-13.
- [69] B. Schultrich, Modeling of ta-C growth: influence of the technological parameters, *Diam. Relat. Mater.* 20 (2011) 785–792.
- [70] O.S. Ishpal, A.K. Panwar, S. Srivastava, R.K. Kumar, M. Tripathi, S. Kumar, Singh, Effect of substrate bias in amorphous carbon films having embedded nanocrystallites, *Surf. Coat. Technol.* 206 (2011) 155–164.
- [71] M.L. Tan, Y.W. Yan, H.Y. Zhang, X. Han, J.Q. Zhu, J.C. Han, H.T. Ma, Corrosion protection of ultra-thin ta-C films for recording slider applications at varied substrate bias, *Surf. Coat. Technol.* 203 (2009) 963–966.
- [72] R.J. Yeo, E. Rismani, N. Dwivedi, D.J. Blackwood, H.R. Tan, Z. Zhang, S. Tripathy, C.S. Bhatia, Bi-level surface modification of hard disk media by carbon using filtered cathodic vacuum arc: reduced overcoat thickness without reduced corrosion performance, *Diam. Relat. Mater.* 44 (2014) 100–108.
- [73] X.C. Chen, Z.J. Peng, X. Yu, Z.Q. Fu, W. Yue, C.B. Wang, Microstructure and tribological performance of self-lubricating diamond/tetrahedral amorphous carbon composite film, *Appl. Surf. Sci.* 257 (2011) 3180–3186.
- [74] R.G. Lacerda, P. Hammer, F.L. Freire Jr., F. Alvarez, F.C. Marques, On the structure of argon assisted amorphous carbon films, *Diam. Relat. Mater.* 9 (2000) 796–800.
- [75] L. Han, D. Liu, X. Chen, L. Yang, Y. Zhao, The deposition of a thick tetrahedral amorphous carbon film by argon ion bombardment, *Appl. Surf. Sci.* 258 (2012) 4794–4800.
- [76] C.K. Chung, C.C. Peng, B.H. Wu, T.S. Chen, Residual stress and hardness behaviors of the two-layer C/Si films, *Surf. Coat. Technol.* 202 (2007) 1149–1153.
- [77] S. Makowski, F. Schaller, V. Weinhacht, G. Englberger, M. Becker, Tribochemical induced wear and ultra-low friction of superhard ta-C coatings, *Wear* 392–393 (2017) 139–151.
- [78] L.L. Ru, J.J. Huang, L. Gao, B. Qi, Hydrogen-free diamond-like carbon films prepared by microwave electron cyclotron resonance plasma-enhanced direct current magnetron sputtering, *Thin Solid Films* 519 (2010) 86–90.
- [79] O. Takai, V. Anita, N. Saito, Properties of DLC thin films produced by RF PE-CVD from pyrrole monomer, *Surf. Coat. Technol.* 200 (2005) 1106–1109.
- [80] K.H. Lai, C.Y. Chan, M.K. Fung, I. Bello, C.S. Lee, S.T. Lee, Mechanical properties of DLC films prepared in acetylene and methane plasmas using electron cyclotron resonance microwave plasma chemical vapor deposition, *Diam. Relat. Mater.* 10 (2001) 1862–1867.
- [81] C.A. Charitidis, Nanomechanical and nanotribological properties of carbon-based thin films: a review, *Int. J. Refract. Met. H.* 28 (2010) 51–70.
- [82] A. Leyland, A. Matthews, On the significance of the H/E ratio in wear control: a nanocomposite coating approach to optimised tribological behavior, *Wear* 246 (2000) 1–11.
- [83] S. Zhang, D. Sun, Y. Fu, H. Du, Toughening of hard nanostructural thin films: a critical review, *Surf. Coat. Technol.* 198 (2005) 2–8.
- [84] M. Haršáni, N. Ghafoor, K. Calamba, P. Zacková, M. Sahl, T. Vopát, L. Satrapinskyy, M. Čaplovičová, L. Čaplovič, Adhesive-deformation relationships and mechanical properties of nc-AlCrN/a-SiNx hard coatings deposited at different bias voltages, *Thin Solid Films* 650 (2018) 11–19.
- [85] J. Li, S. Zhang, M. Li, Influence of the C₂H₂ flow rate on gradient TiCN films deposited by multi-arc ion plating, *Appl. Surf. Sci.* 283 (2013) 134–144.
- [86] B. Warcholinski, A. Gilewicz, T.A. Kuznetsova, T.I. Zubar, S.A. Chizhik, S.O. Abetkovskaia, V.A. Lapitskaya, Mechanical properties of Mo(C)N coatings deposited using cathodic arc evaporation, *Surf. Coat. Technol.* 319 (2017) 117–128.
- [87] Y. Wang, L. Wang, G. Zhang, S.C. Wang, R.J.K. Wood, Q. Xue, Effect of bias voltage on microstructure and properties of Ti-doped graphite-like carbon films synthesized by magnetron sputtering, *Surf. Coat. Technol.* 205 (2010) 793–800.
- [88] L. Cui, Z. Lu, L. Wang, Environmental effect on the load-dependent friction behavior of a diamond-like carbon film, *Tribol. Int.* 82 (2015) 195–199.
- [89] Z. Li, X. Guan, Y. Wang, J. Li, X. Cheng, X. Lu, L. Wang, Q. Xue, Comparative study on the load carrying capacities of DLC, GLC and CrN coatings under sliding-friction condition in different environments, *Surf. Coat. Technol.* 321 (2017) 350–357.
- [90] F. Cheng, Junpin Lin, Y. Liang, Friction and wear properties of a high Nb-containing TiAl alloy against WC₈Co, Si₃N₄, and GCr15 in an unlubricated contact, *Intermetallics* 106 (2019) 7–12.
- [91] Y. Kong, X. Tian, C. Gong, D.A. Golosov, M. Li, Q. Tian, Enhanced discharge and surface properties of (Ti,Al)CrN coatings by cleaning cathodic-arc chamber, *Surf. Coat. Technol.* 366 (2019) 41–53.
- [92] D. He, L. Shang, Z. Lu, G. Zhang, L. Wang, Q. Xue, Tailoring the mechanical and tribological properties of B₄C/a-C coatings by controlling the boron carbide content, *Surf. Coat. Technol.* 329 (2017) 11–18.